

Measurements of Charged Kaon Semileptonic Decay Branching Fractions $K^\pm \rightarrow \pi^0 \mu^\pm \nu$ and $K^\pm \rightarrow \pi^0 e^\pm \nu$ and Their Ratio

J.R. Batley, C. Lazzeroni, D.J. Munday, M.W. Slater, S.A. Wotton

*Cavendish Laboratory, University of Cambridge, Cambridge, CB3 0HE, U.K.*¹⁾

R. Arcidiacono²⁾, G. Bocquet, N. Cabibbo, A. Ceccucci, D. Cundy³⁾, V. Falaleev,
M. Fidecaro, L. Gatignon, A. Gonidec, W. Kubischta, A. Norton⁴⁾, M. Patel, A. Peters

CERN, CH-1211 Geneva 23, Switzerland

S. Balev, P.L. Frabetti, E. Goudzovski, P. Hristov⁵⁾, V. Kekelidze⁵⁾, V. Kozhuharov,
L. Litov, D. Madigozhin, E. Marinova, N. Molokanova, I. Polenkevich, Yu. Potrebenikov,
S. Stoynev⁶⁾, A. Zinchenko

Joint Institute for Nuclear Research, Dubna, Russian Federation

E. Monnier⁷⁾, E. Swallow, R. Winston

The Enrico Fermi Institute, The University of Chicago, Chicago, IL 60126, U.S.A.

P. Rubin, A. Walker

*Department of Physics and Astronomy, University of Edinburgh,
JCMB King's Buildings, Mayfield Road, Edinburgh, EH9 3JZ, U.K.*

W. Baldini, A. Cotta Ramusino, P. Dalpiaz, C. Damiani, M. Fiorini, A. Gianoli,
M. Martini, F. Petrucci, M. Savrié, M. Scarpa, H. Wahl

Dipartimento di Fisica dell'Università e Sezione dell'INFN di Ferrara, I-44100 Ferrara, Italy

A. Bizzeti⁸⁾, M. Calvetti, E. Celeghini, E. Iacopini, M. Lenti, F. Martelli⁹⁾,
G. Ruggiero⁵⁾, M. Veltri⁹⁾

Dipartimento di Fisica dell'Università e Sezione dell'INFN di Firenze, I-50125 Firenze, Italy

M. Behler, K. Eppard, K. Kleinknecht, P. Marouelli, L. Masetti, U. Moosbrugger,
C. Morales Morales, B. Renk, M. Wache, R. Wanke, A. Winhart
*Institut für Physik, Universität Mainz, D-55099 Mainz, Germany*¹⁰⁾

D. Coward¹¹⁾, A. Dabrowski, T. Fonseca Martin⁵⁾, M. Shieh, M. Szleper, M. Velasco,
M.D. Wood¹²⁾

*Department of Physics and Astronomy, Northwestern University,
Evanston, IL 60208-3112, U.S.A.*

G. Anzivino, P. Cenci, E. Imbergamo, M. Pepe, M.C. Petrucci, M. Piccini⁵⁾, M. Raggi,
M. Valdata-Nappi

Dipartimento di Fisica dell'Università e Sezione dell'INFN di Perugia, I-06100 Perugia, Italy

C. Cerri, G. Collazuol, F. Costantini, L. DiLella, N. Doble, R. Fantechi, L. Fiorini¹³⁾,
S. Giudici, G. Lamanna, I. Mannelli, A. Michetti, G. Pierazzini, M. Sozzi

*Dipartimento di Fisica, Scuola Normale Superiore e Sezione dell'INFN di Pisa,
I-56100 Pisa, Italy*

B. Bloch-Devaux, C. Cheshkov⁵⁾, J.B. Chèze, M. De Beer, J. Derré, G. Marel,
E. Mazzucato, B. Peyaud, B. Vallage

DSM/DAPNIA - CEA Saclay, F-91191 Gif-sur-Yvette, France

M. Holder, A. Maier⁵⁾, M. Ziolkowski
Fachbereich Physik, Universität Siegen, D-57068 Siegen, Germany¹⁴⁾

S. Bifani, C. Biino, N. Cartiglia, M. Clemencic⁵⁾, S. Goy Lopez, F. Marchetto
*Dipartimento di Fisica Sperimentale dell'Università e Sezione dell'INFN di Torino,
I-10125 Torino, Italy*

H. Dibon, M. Jeitler, M. Markytan, I. Mikulec, G. Neuhofer, L. Widhalm
*Österreichische Akademie der Wissenschaften, Institut für Hochenergiephysik,
A-10560 Wien, Austria¹⁵⁾*

Submitted for publication in European Physics Journal C

¹⁾ Funded by the U.K. Particle Physics and Astronomy Research Council

²⁾ Present address: Dipartimento di Fisica Sperimentale dell'Università Sezione dell'INFN di Torino, I-10125 Torino, Italy

³⁾ Present address: Istituto di Cosmogeofisica del CNR di Torino, I-10133 Torino, Italy

⁴⁾ Present address: Dipartimento di Fisica dell'Università e Sezione Ferrara, I-44100 Ferrara, Italy

⁵⁾ Present address: CERN, CH-1211 Geneva 23, Switzerland

⁶⁾ Present address: Department of Physics and Astronomy, Northwestern University, Evanston, IL 60208-3112, U.S.A.

⁷⁾ Also at Centre de Physique des Particules de Marseille, IN2P3-CNRS, Université de la Méditerranée, Marseille, France

⁸⁾ Also Dipartimento di Fisica, Università di Modena, I-41100 Modena, Italy

⁹⁾ Istituto di Fisica, Università di Urbino, I-61029 Urbino, Italy

¹⁰⁾ Funded by the German Federal Minister for Education and research under contract 05HK1UM1/1

¹¹⁾ Permanent address: SLAC, Stanford University, Menlo Park, CA 94025, U.S.A.

¹²⁾ Present address: UCLA, Los Angeles, CA 90024, U.S.A.

¹³⁾ Present address: Institut de Física d'Altes Energies, Universitat A Barcelona, E-08193 Bellaterra (Barcelona), Spain

¹⁴⁾ Funded by the German Federal Minister for Research and Technology (BMBF) under contract 056SI74

¹⁵⁾ Funded by the Austrian Ministry for Traffic and Research under the contract GZ 616.360/2-IV GZ 616.363/2-VIII, and by the Fonds für Wissenschaft und Forschung FWF Nr. P08929-PHY

Abstract

Measured ratios of decay rates for $\mathcal{R}_{Ke3/K2\pi}$, $\mathcal{R}_{K\mu3/K2\pi}$ and $\mathcal{R}_{K\mu3/Ke3}$ are presented. These measurements are based on K^\pm decays collected in a dedicated run in 2003 by the NA48/2 experiment at CERN. The results obtained are $\mathcal{R}_{Ke3/K2\pi} = 0.2496 \pm 0.0009(stat) \pm 0.0004(syst)$ and $\mathcal{R}_{K\mu3/K2\pi} = 0.1637 \pm 0.0006(stat) \pm 0.0003(syst)$. Using the PDG average for the $K^\pm \rightarrow \pi^\pm \pi^0$ normalisation mode, both values are found to be larger than the current values given by the Particle Data Book and lead to a larger magnitude of the $|V_{us}|$ CKM element than previously accepted. When combined with the latest Particle Data Book value of $|V_{ud}|$, the result is in agreement with unitarity of the CKM matrix. In addition, a new measured value of $\mathcal{R}_{K\mu3/Ke3} = 0.656 \pm 0.003(stat) \pm 0.001(syst)$ is compared to the semi-empirical predictions based on the latest form factor measurements.

1 Introduction

New measurements of the charged kaon semileptonic decays, $K^\pm \rightarrow \pi^0 e^\pm \nu$ (K_{e3}) and $K^\pm \rightarrow \pi^0 \mu^\pm \nu$ ($K_{\mu3}$), are presented. These measurements are based on K^\pm decays collected in 2003 by the NA48/2 Collaboration at the CERN SPS.

The measured ratios are:

$$\mathcal{R}_{Ke3/K2\pi} \equiv \frac{\Gamma(K^\pm \rightarrow \pi^0 e^\pm \nu)}{\Gamma(K^\pm \rightarrow \pi^\pm \pi^0)}, \quad \mathcal{R}_{K\mu3/K2\pi} \equiv \frac{\Gamma(K^\pm \rightarrow \pi^0 \mu^\pm \nu)}{\Gamma(K^\pm \rightarrow \pi^\pm \pi^0)} \quad (1)$$

and

$$\mathcal{R}_{K\mu3/Ke3} \equiv \frac{\Gamma(K^\pm \rightarrow \pi^0 \mu^\pm \nu)}{\Gamma(K^\pm \rightarrow \pi^0 e^\pm \nu)}. \quad (2)$$

In both the numerator and denominator, the decays contain a charged track and at least two photons originating from a π^0 decay, thus leading to a partial cancellation in the acceptance and reconstruction uncertainties. Contributions from internal bremsstrahlung are included for all three decay modes. The general reconstruction methods are the same for all three measurements but the event selection varies because different particle identification criteria are applied.

The main interest in measuring these quantities is to extract: (1) the individual semileptonic decay widths needed to determine the V_{us} element in the Cabibbo-Kobayashi-Maskawa (CKM) quark mixing matrix; and (2) the ratio $\Gamma(K_{\mu3})/\Gamma(K_{e3})$ which is a function of the slope parameters of the form factors. On the assumption of $\mu - e$ universality this ratio provides a consistency check between measurements of the form factors and of the partial decay widths.

This paper is organized as follows. Section 2 outlines the phenomenological description of semileptonic decays. The experimental setup is described in Section 3. The event selection and all corrections applied to the data are presented in Section 4. Section 5 includes a detailed description of the acceptance corrections and radiative effects. Finally, the results are presented in Section 6, and their comparison with theory and their impact on V_{us} are given in Section 7.

2 Decay rates for semileptonic decays

The decay rate for charged semileptonic decays can be written as follows [1]:

$$\Gamma(K_{\ell3}) = \frac{G_F^2}{384\pi^3} m_K^5 S_{EW} |V_{us}|^2 |f_+(0)|^2 I_K^\ell (1 + \delta_K^\ell) \quad , \quad (3)$$

where ℓ refers to either e or μ , G_F is the Fermi constant, m_K is the kaon mass, S_{EW} is the short-distance radiative correction, $(1 + \delta_K) \simeq (1 + \delta_{SU(2)}^\ell + \delta_{EM}^\ell)^2$ is the model-dependent long-distance correction with contributions due to isospin breaking in strong ($SU(2)$) and electromagnetic (EM) interactions, $f_+(0)$ is the form factor at zero momentum transfer ($t = 0$) for the $\ell\nu$ system. The remaining term, I_K^ℓ , is the result of the phase space integration after factoring out $f_+(0)$, and is defined as [1]:

$$I_K^\ell = \frac{1}{m_K^8} \int_{m_\ell^2}^{(m_K - m_\pi)^2} \frac{dt}{2t^3} (t - m_\ell^2)^2 T^{1/2}(t, m_K^2, m_\pi^2) \\ \times \left\{ T(t, m_K^2, m_\pi^2) (2t + m_\ell^2) |f_+(t)/f_+(0)|^2 + 3m_\ell^2 (m_K^2 - m_\pi^2)^2 |f_0(t)/f_+(0)|^2 \right\}, \quad (4)$$

where $T(x, y, z) \equiv x^2 + y^2 + z^2 - 2xy - 2xz - 2yz$, and m_π and m_ℓ are the masses of the π^0 and the charged lepton, respectively. The two form factors correspond to the angular momentum configuration of the $K - \pi$ system, with $f_+(t)$ representing the vector form factor, while $f_0(t)$ is the scalar form factor. The t dependence of the form factors can be described using a quadratic (linear) approximation for the vector (scalar) term:

$$f_+(t) = f_+(0) \left(1 + \lambda'_+ \frac{t}{m_{\pi^\pm}^2} + \frac{1}{2} \lambda''_+ \frac{t^2}{m_{\pi^\pm}^4} \right) \quad \text{and} \quad f_0(t) = f_+(0) \left(1 + \lambda_0 \frac{t}{m_{\pi^\pm}^2} \right), \quad (5)$$

where $f_+(0)$ is obtained from theory, and λ'_+ , λ''_+ and λ_0 are measured [2]. The second term in I_K^ℓ shows that $K_{\mu 3}$ decays are more sensitive to the scalar form factor than $K_{e 3}$.

Other ways to describe the momentum dependence of the form factors are also considered and discussed in Section 5.

Assuming $\mu - e$ universality, the $\Gamma(K_{\mu 3})/\Gamma(K_{e 3})$ ratio is predicted to be [3]:

$$\mathcal{R}_{K_{\mu 3}/K_{e 3}} \equiv \Gamma(K_{\mu 3})/\Gamma(K_{e 3}) = \frac{0.645 + 2.087\lambda_+ + 1.464\lambda_0 + 3.375\lambda_+^2 + 2.573\lambda_0^2}{1 + 3.457\lambda_+ + 4.783\lambda_+^2}. \quad (6)$$

This semi-empirical formula assumes a linear approximation for the form factors, $f_{+,0}(t) = f_+(0)(1 + \lambda_{+,0} \frac{t}{m_{\pi^\pm}^2})$.

If the assumption of $\mu - e$ universality is removed, Eq. (3) implies that:

$$\mathcal{R}_{K_{\mu 3}/K_{e 3}} = [g_\mu f_+^\mu(0)/g_e f_+^e(0)]^2 \times (I_K^\mu(1 + \delta_K^\mu))/(I_K^e(1 + \delta_K^e)). \quad (7)$$

where g is the weak coupling constant for the lepton current. The $(1 + \delta_K^e)/(1 + \delta_K^\mu)$ ratio for charged kaons is very close to unity because the δ_K^ℓ 's are dominated by the few percent $SU(2)$ correction that is in common between the electron and the muon channel. The EM corrections are at the per mille level and compatible with zero within errors [4, 5, 6]. This is not necessarily true for neutral kaons because there is no $SU(2)$ correction and also the electromagnetic correction for the muons is larger.

3 Experimental setup

3.1 Beam

The experiment uses simultaneous K^+ and K^- beams produced by 400 GeV protons impinging on a Be target. The beam has particles of opposite charge with a central momentum of 60 GeV/c and a momentum band of $\pm 3.8\%$ produced at zero angle. Both

beams are selected by a system of dipole magnets forming an achromat, along with focusing quadrupoles, muon sweepers and collimators. The spill length is about 4.5s out of a 16.8s cycle time, and the proton intensity is fairly constant during the spill with a mean of 5×10^{10} protons per spill. The positive (negative) kaon flux at the entrance of the decay volume is 3.2×10^6 (1.8×10^6) particles per spill.

For the measurements presented here, the proton beam intensity is reduced from its nominal value so that the data-acquisition system can handle the rate of the minimum bias trigger. The $K^+/K^- \simeq 1.78$ flux ratio is given by their production rate at the Be-target.

3.2 Detector

The final beam collimator is immediately followed by a 114m long cylindrical tank, which is evacuated in order to minimize the interactions of the decay products. The tank is terminated by a 0.3% radiation length (X_0) thick Kevlar window, except in a region close to the beam which continues in a vacuum pipe through the centre of the downstream detectors. The detector is located downstream of this Kevlar window.

The tracking is performed with a spectrometer housed in a helium gas volume. It consists of two drift chambers before and two after a dipole magnet with a horizontal transverse momentum kick of 120 MeV/c. Each chamber has four views, each of which has two sense wire planes. The resulting space points are typically reconstructed with a resolution of 150 μm in each projection. The momentum resolution of the spectrometer is $\sigma_p/p = 1.02\% \oplus 0.044\% \cdot p$, where p is in GeV/c. The track time resolution is 1.4 ns.

The detection and measurement of electromagnetic showers are performed with a 27 X_0 -deep liquid krypton calorimeter (LKr) that has an energy resolution[7] of $\sigma(E)/E = 3.2\%/\sqrt{E} \oplus 9\%/E \oplus 0.42\%$, where E is in GeV. The calorimeter is subdivided into 13248 cells of transverse dimension 2 cm \times 2 cm.

The reconstructed kaon mass in $K^\pm \rightarrow \pi^\pm \pi^0$ ($K_{2\pi}$) decays has a typical resolution of 3.25 ± 0.05 MeV/c², without imposing the π^0 mass constraint.

A scintillator hodoscope is located between the spectrometer and the LKr for triggering purposes. It consists of two planes, segmented in horizontal and vertical strips respectively, with each plane arranged in four quadrants. The time resolution for the hodoscope system is 200 ps.

Downstream of the LKr calorimeter is an iron-scintillator sandwich hadron calorimeter (HAC), followed by muon counters (MUC) which consist of three planes of plastic scintillators shielded by the HAC and a 80 cm thick iron wall. The first two planes are made of 25 cm wide horizontal and 25 cm wide vertical scintillator strips, with a length of 2.7 m. The third plane consists of horizontal strips of width 44.6 cm and is mainly used to measure the efficiency of the counters in the first two planes. The central strip in each plane is split with a gap of 21 cm to accommodate the beam pipe. The fiducial volume of the experiment is principally determined by the LKr calorimeter acceptance.

3.3 Trigger and readout

The data coming from the detector is sampled every 25 ns, and eight samples are recorded in time windows of 200 ns.

The trigger selection is defined by at least one hit in each of the horizontal and vertical planes of the hodoscope, within the same quadrant. The typical rate of this trigger at the reduced intensity is 1.3×10^5 per burst, and is downscaled by a factor of four in order to match the allowed limit of the data-acquisition system of 50000 events per burst. The efficiency of this trigger for events containing one track is calculated from

events collected by requiring at least three hit wires in at least three views of the upstream chamber recorded within 200 ns. As shown in Table 1, the trigger efficiency is found to be high and independent of the decay mode and the type of kaon beamline.

4 Event selection and reconstruction

The signals for the K_{e3} , $K_{\mu3}$ and $K_{2\pi}$ decay modes require one track in the drift chambers and at least two clusters (photons) in the LKr that are consistent with a π^0 decay. It is an important feature of this analysis that their basic event reconstruction and selection criteria are the same. These decay modes are separated from each other on the basis of particle identification and additional kinematic requirements, which also serves to reduce the background to a negligible level.

4.1 Common selection criteria for K_{e3} , $K_{\mu3}$ and $K_{2\pi}$

All events are required to have at least one track that satisfies the following conditions:

- the track must be at least 15 cm away from the center of each drift chambers and at least 15 cm from the center of the LKr, 11 cm from its outside borders, and 2 cm from any inefficient cell;
- to be within the allowed 37 ns readout window defined by the trigger hodoscopes;
- to pass all track quality requirements.

The decay vertex, $V_{x,y,z}$, is reconstructed from the charged track and the beam axis. After correcting for residual magnetic fields inside the decay pipe, it is required that:

- the longitudinal position, V_z , must be 1316 cm downstream of the final beam collimator, and 2584 cm upstream from the end of the decay pipe, for a total of 75 m of decay volume;
- the transverse position, $V_{x,y}$, must be within three sigma (around 2.5 cm) in x and y from the beam axis. The actual cut depends on the longitudinal vertex position due to the varying uncertainty of the extrapolation to the vertex position.

All cluster candidates in the π^0 reconstruction need to be clearly identified as photons, that is:

- the energy of the cluster is greater than 3 GeV and less than 65 GeV;
- time difference between clusters is smaller than 5 ns;
- the minimum distance between clusters is 10 cm in order to minimize the effect of energy sharing on cluster reconstruction;
- the minimum distance between clusters and extrapolated tracks is greater than 10 (35) cm, so that no charged lepton (hadron) track is associated to the clusters.

To make an inclusive measurement of the radiation, a minimum of two reconstructed photons is required. The threshold to define a reconstructed photon, 3 GeV, leads to a high fraction of the events with only two photons reconstructed. The fraction of events with at least one extra cluster in the calorimeter is 2.3% in the case of K_{e3} , 0.3% in $K_{\mu3}$ and 10% in $K_{2\pi}$. Fig. 1 shows the invariant mass distribution for these two photon events reconstructed using the V_z component of the charged vertex. The non-Gaussian tails are of the same order in all three channels. No requirement on the $\gamma\gamma$ invariant mass is made.

For the small fraction of events with extra clusters, the best π^0 candidate is selected by comparing the V_z component of the charged vertex and the longitudinal vertex, z_π , of the π^0 . This neutral vertex is reconstructed by assuming the π^0 mass and using the kinematical information from the two photon candidates in the $\pi^0 \rightarrow \gamma\gamma$ decay. z_π is

calculated from the distance, d_π , of the π^0 vertex to the LKr calorimeter calculated from:

$$d_\pi = \sqrt{E_i E_j [(x_i - x_j)^2 + (y_i - y_j)^2]} / m_{\pi^0}, \quad (8)$$

where x_i and y_i are the coordinates of the impact point of a the i^{th} γ in the LKr, and E_i is the energy of the corresponding γ . The longitudinal vertex position, z_π , is given by $z_\pi = z$ (LKr position) $- d_\pi$. Although there is no explicit requirement on $V_z - z_\pi$, the combination with the smallest $V_z - z_\pi$ is taken.

4.2 Selection criteria to distinguish between K_{e3} , $K_{\mu3}$ and $K_{2\pi}$

The invariant mass for the $K_{2\pi}$ candidates is required to be within three sigma of the reconstructed K^\pm mass, that is:

$$0.4772 \text{ GeV}/c^2 < m_{\pi^\pm\pi^0} < 0.5102 \text{ GeV}/c^2,$$

while for $K_{\ell3}$ candidates:

$$m_{\pi^\pm\pi^0} < 0.4772 \text{ GeV}/c^2 \quad \text{or} \quad m_{\pi^\pm\pi^0} > 0.5102 \text{ GeV}/c^2,$$

assuming m_{π^\pm} instead of m_ℓ . The Monte Carlo simulated reconstructed invariant mass for the track and the π^0 , without applying particle identification and under the assumption that the track is a π^\pm , is shown in Fig. 2 for the relevant decay channels.

The allowed range in the transverse momentum of the track, P_T , with respect to the beam axis is required to be:

$$K_{e3} : P_T < 0.200 \text{ GeV}/c, \quad K_{\mu3} : P_T < 0.200 \text{ GeV}/c, \quad K_{2\pi} : P_T < 0.215 \text{ GeV}/c.$$

The missing mass squared, m_ν^2 , is reconstructed under the assumption that the kaon energy is 60 GeV. The allowed m_ν^2 range for each channel is:

$$\begin{aligned} K_{e3} : & \quad -0.012 \text{ GeV}^2/c^4 < m_\nu^2 < 0.012 \text{ GeV}^2/c^4, \\ K_{\mu3} : & \quad -0.010 \text{ GeV}^2/c^4 < m_\nu^2 < 0.010 \text{ GeV}^2/c^4, \\ K_{2\pi} : & \quad -0.0025 \text{ GeV}^2/c^4 < m_\nu^2 < 0.001 \text{ GeV}^2/c^4, \end{aligned}$$

in order to distinguish between events that are consistent with a three body or a two body decay, see Fig. 3.

4.3 Additional selection criteria for K_{e3} candidates

The additional requirements for this channel are: (1) the electron identification is performed by combining the calorimeter energy measurement (E) with the spectrometer momentum (p), and requiring $E/p > 0.95$. The average electron identification efficiency is $(97.37 \pm 0.09)\%$, and the efficiency as a function of p is shown in Fig. 4. The error shown for the electron identification is only statistical in nature, but the systematic uncertainty is expected to be small since the result is reproduced using Dalitz decays; (2) a minimum momentum of 5 GeV/c is required, in order to avoid low particle identification efficiency, and a maximum momentum of 35 GeV/c is also applied to avoid regions of very low rate; (3) the electron and the π^0 energies in the kaon center of mass are required to be less than 0.22 GeV and 0.27 GeV respectively, to further reduce the background from $K_{2\pi}$; and (4) $m_{\mu\pi^0} < 0.425 \text{ GeV}/c^2$ is also required in order to further reduce the $\pi^\pm\pi^0$ background.

Using Monte Carlo simulations, the backgrounds to this channel are found to be well below the per mille level, see Table 2 and Fig. 3(a). The main contribution comes from decays with a π^0 and a π^\pm that pass the E/p requirement; for example, from $K_{2\pi}$ that has a branching fraction that is about four times larger, and $K_{\pi^\pm\pi^0\pi^0}$ where only the information from two of the photons are used.

4.4 Additional selection criteria for $K_{\mu 3}$ candidates

The additional requirements for this channel are: (1) in order to identify a muon a charged track, reconstructed in the spectrometer, is extrapolated to the MUC planes and associated with the MUC hits after testing the spatial separation and time difference between this extrapolated track and the MUC hits. Multiple scattering is taken into account before applying the spatial cut, and light propagation along the MUC strips is taken into account before applying the time-difference cut. A track is classified as a muon if the following conditions are satisfied:

- each track has hits in planes one and two of the MUC;
- for each track, the time difference measured by the chambers or the hodoscope, and by the muon detector does not differ by more than 4.5 ns;

Using these requirements, the efficiency for muon identification is measured from a kinematically selected sample of $K \rightarrow \mu\nu$ and found to be larger than 0.995 as shown in Fig. 5. The average muon identification efficiency is $(99.759 \pm 0.003)\%$. The error shown for the muon identification is only statistical in nature, but the systematic uncertainty is expected to be small since the result is reproduced using data taken with a dedicated muon beam; (2) The individual track momenta is required to be above 10 GeV/c and below 40 GeV/c; (3) the energy of the muon in the kaon center of mass is below 0.23 GeV; (4) the π^0 energy in the kaon center of mass is below 0.23 GeV or $m_{\mu\pi^0} < 0.38$ GeV/c²; and (5) the π^0 energy is smaller than 40 GeV to reduce the background from $K_{2\pi}$.

Backgrounds to this channel are found to be at the two per mille level, see Table 2 and Fig. 3(b). The main contribution comes from decays with a π^0 together with a π^\pm that decays in flight.

4.5 Additional selection criteria for $K_{2\pi}$ candidates

The additional requirements for this channel are: (1) muons are not rejected to avoid losing events where the pion decays (this corresponds to 1.6% of the $K_{2\pi}$ events), but electrons are rejected by requiring $E/pc < 0.95$. The average pion identification efficiency is $(99.524 \pm 0.009)\%$. The fraction of surviving pions after this requirement is shown in Fig. 4(b). The error shown for the pion identification is only statistical in nature, but the systematic uncertainty is expected to be small since the result at low momenta is reproduced using an independent sample of $\pi^\pm\pi^\pm\pi^\mp$ decays. (2) The individual track momenta are required to be above 10 GeV/c and below 50 GeV/c.

Backgrounds to this channel are found to be at the few per mille level, see Table 2. The main contribution is from $K_{\mu 3}$ because we do not reject events with muons.

4.6 Final data samples

Around 56K (31K), 49K (28K) and 462K (256K) events are found for K_{e3}^+ (K_{e3}^-), $K_{\mu 3}^+$ ($K_{\mu 3}^-$) and $K_{2\pi}^+$ ($K_{2\pi}^-$) candidates respectively, after all the event selection requirements are applied (see Table 1).

5 Acceptance calculations

To obtain the acceptance and an estimate of the background fractions, a GEANT[8] based Monte Carlo simulation is modeled for each beam separately. The beam optics for the K^+ and the K^- beamlines are described using TURTLE [9], and fine tuned using fully reconstructed $\pi^\pm\pi^\pm\pi^\mp$ and $\pi^\pm\pi^0$ events.

The main inputs needed to describe the decay amplitude for semileptonic decays are: (1) the radiative corrections, and (2) the parameters, λ'_+ , λ''_+ and λ_0 , of the model

presented in Eq. (5) and used to describe the dependence of the form factors, f_+ and f_0 , on the momentum transferred to the leptons, t ; see Section 2.

In order to reduce the uncertainties due to radiative effects, after identifying the track and the π^0 , events with extra photons are kept. Nevertheless, it is important that the Monte Carlo includes a well defined fraction of radiative decays (like $K_{e3\gamma}$) in order to obtain an acceptance correction that is accurate at the percent level. For example, studies show that ignoring the radiative events in the K_{e3} generation causes the acceptance to be overestimated by 1.6%, even after correcting for virtual effects on the three-body Dalitz plane region using the prescription given in [5].

The PHOTOS package [10] is used to simulate bremsstrahlung, and calculations from [5] are added to include virtual photons and electrons. Figure 6(a) shows a comparison between data and Monte Carlo events for the electron energy in the center of mass of the kaon. Good agreement is found, even though this distribution is sensitive to radiative effects. All other kinematic distributions show that the data are well described by the Monte Carlo after including effects introduced by $K_{e3\gamma}$ events. For example, the invariant mass of the electron and π^0 pair is sensitive to $K_{e3\gamma}$, see Fig. 7. The proper description of the low mass region proved to be sensitive to the inclusion of the $K_{e3\gamma}$. The effect of radiative corrections to the K_{e3} acceptance is confirmed using the program described in reference [11] that includes virtual corrections and the corresponding radiative decay simultaneously. The $K_{e3}^+(K_{e3}^-)$ acceptance is found to be 0.0709 ± 0.0001 (0.0706 ± 0.0001).

For $K_{\mu3}$, the prescription given in [5] is sufficient due to the smaller bremsstrahlung contribution, and adding PHOTOS had a negligible impact on the acceptance. Fig. 6(b) shows a comparison between data and Monte Carlo events for the muon energy in the center of mass of the kaon. The $K_{\mu3}^+(K_{\mu3}^-)$ acceptance is found to be 0.0930 ± 0.0001 (0.0927 ± 0.0001).

For a similar reason, the change in acceptance in $K_{2\pi}$ is found to be smaller than one per mille if the radiative events are included in the generator. The $K_{2\pi}^+(K_{2\pi}^-)$ acceptance is found to be 0.1424 ± 0.0001 (0.1419 ± 0.0001).

The response of the LKr detector, even though simulated, is not used for particle identification during the acceptance calculations. The particle identification efficiency is studied using data and corrections are made separately, see Fig. 4 and 5. The acceptances after including the corrections due to particle identification for all three decay modes are summarized in Table 1, and the assigned uncertainties are statistical in nature.

The acceptance for K^+ is systematically higher than for K^- due to differences introduced by the polarity selected for the spectrometer magnet.

5.1 Form factor description in the Monte Carlo generation

The Dalitz distributions for the semileptonic decays are generated with: $\lambda'_+ = 0.02485 \pm 0.00163 \pm 0.00034$, $\lambda''_+ = 0.00192 \pm 0.00062 \pm 0.00071$ (both from K_{e3} decays) [2], and $\lambda_0 = 0.0196 \pm 0.0012$ (assuming $\mu - e$ universality) [2]. The change in acceptance when the current values of λ'_+ , λ''_+ and λ_0 are changed by one sigma is about 0.08% (0.07%) for K_{e3} ($K_{\mu3}$). The correlation between λ'_+ and λ''_+ is assumed to be -0.95 [2], while the measurements for the vector and the scalar form factor parameters are assumed to be uncorrelated. Table 3 shows the the resulting slope in the $\mathcal{R}_{K_{e3}/K_{2\pi}}$, $\mathcal{R}_{K_{\mu3}/K_{2\pi}}$ and $\mathcal{R}_{K_{\mu3}/K_{e3}}$ measurements after changing form factor parameter by \pm one sigma, while maintaining the other parameters constant. The contribution from this change in acceptance to the total systematic error is included in Table 4.

The changes in acceptance due to alternative models describing the t dependence

of the form factors are given below:

- the linear approximation:

$$f_{+,0}(t) = f_+(0) \left(1 + \lambda_{+,0} \frac{t}{m_{\pi^\pm}^2} \right), \quad (9)$$

where $\lambda_+ = 0.0296 \pm 0.0008$ and $\lambda_0 = 0.0196 \pm 0.0012$ (assuming $\mu - e$ universality) [2]. In this case, the ratio between the acceptance obtained using this approximation compared to the acceptance using the quadratic approximation (Eq. 5) is found to be 1.0006 and 0.9998 for K_{e3} and $K_{\mu3}$, respectively.

- the pole approximation:

$$f_{+,0}(t) = f_+(0) \left(\frac{m_{V,S}^2}{m_{V,S}^2 - t} \right), \quad (10)$$

where $m_V = 0.877 \pm 0.005 \text{ GeV}/c^2$ for K_{e3}^0 and $K_{\mu3}^0$ (assuming $\mu - e$ universality) [2] and $m_S = 1.187 \pm 0.050 \text{ GeV}/c^2$ for $K_{\mu3}^0$ (assuming $\mu - e$ universality) [2]. These pole masses are obtained from neutral kaons. In this case, the ratio between the acceptance obtained using this approximation compared to the acceptance using the quadratic approximation (Eq. 5) is found to be 0.9996 and 0.9984 for K_{e3} and $K_{\mu3}$, respectively.

The full difference in acceptance between the pole approximation and the quadratic approximation is assigned as an uncertainty due to the choice of form factor model, see Table 4.

6 Result

Table 1 lists all quantities needed to evaluate \mathcal{R}_{K_i/K_j} :

$$\mathcal{R}_{K_i/K_j} = \frac{Acc_{K_j} \times \epsilon_{track_{1D_j}} \times Trig_{K_j} \times N_{K_i} \times (1 + \Delta_{K_j})}{Acc_{K_i} \times \epsilon_{track_{1D_i}} \times Trig_{K_i} \times N_{K_j} \times (1 + \Delta_{K_i})}, \quad (11)$$

where $i, j = \ell 3, 2\pi$. The correction to K_{e3} due to particle identification efficiency ($\epsilon_{track_{1D}}$) amounts to a few percent, while the background correction ($1 + \Delta_{K_i}$) is negligible. $K_{\mu3}$ and $K_{2\pi}$ require a particle identification correction that is below the percent level, and a correction for background correction that is only a few per mille.

The results for K^+ and K^- combined are:

$$\mathcal{R}_{K_{e3}/K_{2\pi}} = 0.2496 \pm 0.0009(stat) \pm 0.0004(syst), \quad (12)$$

$$\mathcal{R}_{K_{\mu3}/K_{2\pi}} = 0.1637 \pm 0.0006(stat) \pm 0.0003(syst), \quad (13)$$

$$\mathcal{R}_{K_{\mu3}/K_{e3}} = 0.656 \pm 0.003(stat) \pm 0.001(syst). \quad (14)$$

The individual K^+ and K^- results and their systematic uncertainties are listed in Table 4. The sources of systematic uncertainties are due to the corrections listed in Table 1 and the treatment of the form factors as discussed in Section 5.1.

The ratios are found to be insensitive to the photon reconstruction and track-finding. Analysis of these ratios as a function of their basic distributions show stability.

The final results are shown in Fig. 8 for $\mathcal{R}_{K_{e3}/K_{2\pi}}$ and $\mathcal{R}_{K_{\mu3}/K_{2\pi}}$, and in Fig. 9 for $\mathcal{R}_{K_{\mu3}/K_{e3}}$. These can be compared to the current PDG values of $\mathcal{R}_{K_{e3}/K_{2\pi}} = 0.238 \pm$

0.004 [2], $\mathcal{R}_{K_{\mu 3}/K_{2\pi}} = 0.159 \pm 0.003$ [12] and $\mathcal{R}_{K_{\mu 3}/K_{e3}} = 0.668 \pm 0.008$ [2]. Taking the current PDG value for the $K_{2\pi}$ branching fraction, 0.2092 ± 0.0012 [2], the branching fractions for the semileptonic decays are found to be:

$$Br(K_{e3}) = 0.05221 \pm 0.00019(stat) \pm 0.00008(syst) \pm 0.00030(norm), \quad (15)$$

$$Br(K_{\mu 3}) = 0.03425 \pm 0.00013(stat) \pm 0.00006(syst) \pm 0.00020(norm). \quad (16)$$

The uncertainty is dominated by the existing data for the $K_{2\pi}$ branching fraction. Recall the corresponding PDG values [2] are $Br(K_{e3}) = 0.0498 \pm 0.0007$ and $Br(K_{\mu 3}) = 0.0332 \pm 0.0006$. Higher branching fractions are found for both K_{e3} and $K_{\mu 3}$, confirming the K_{e3} results reported by the BNL-E865 collaboration [13].

7 Discussion

7.1 V_{us} matrix element

As discussed in Section 2, the measured partial widths for semileptonic decays can be combined with theoretical corrections and other experimental measurements to calculate $|V_{us}|$.

Using the newly measured branching fractions given in Eqs. (15)-(16), the K^\pm lifetime $\tau_{K^+}^{PDG} = (1.2385 \pm 0.0024) \times 10^{-8} s$ [2], $G_F = (1.16637 \pm 0.00001) \times 10^{-5} \text{ GeV}^{-2}$ [14], $m_K = 0.493677 \pm 0.000016 \text{ GeV}/c^2$ [2], $S_{EW} = 1.0230 \pm 0.0003$ [15], and the full phase space integrals and long-distance corrections as given in Table 5, the $|V_{us}|$ matrix element times the vector form factor $f_+(0)$ is found to be (see Eq. (3)):

$$|V_{us}|f_+(0) = 0.2204 \pm 0.0012, \quad [K_{e3}] \quad (17)$$

$$= 0.22040 \pm 0.00039(stat) \pm 0.00016(syst) \pm 0.00062(norm) \pm 0.00095(ext),$$

$$= 0.2177 \pm 0.0013, \quad [K_{\mu 3}] \quad (18)$$

$$= 0.21774 \pm 0.00041(stat) \pm 0.00019(syst) \pm 0.00064(norm) \pm 0.00103(ext),$$

from K_{e3} and $K_{\mu 3}$, respectively. 53% (60%) of the external (*ext*) error is due to the sum of the long-distance corrections, $SU(2)$ and EM corrections, taken from [4, 5, 6] for K_{e3} and $K_{\mu 3}$, respectively. The phase space integral, Eq. (4), is evaluated using the quadratic approximation, Eq. (5), and gives the next largest contribution to the external error. The last significant uncertainty comes from the error in the K^\pm lifetime. Combining these $|V_{us}|f_+(0)$ values by assuming $\mu - e$ universality, we obtain:

$$|V_{us}|f_+(0) = 0.2197 \pm 0.0012, \quad (19)$$

$$|V_{us}| = 0.2289 \pm 0.0013(ther) \pm 0.0019(theo),$$

where “*theo*” refers to the theoretical uncertainty due to $f_+(0)$, and “*other*” refers to all the uncertainties already included in Eqs. (17)-(18) and their correlation. To extract $|V_{us}|$, it is assumed that the value of $f_+(0)$ is 0.961 ± 0.008 [1] as calculated for neutral kaons. There is no need to make a distinction between charged and neutral kaons in $f_+(0)$ because the $SU(2)$ correction is applied directly, see Eq. (3)-(4) and Table 5.

These $|V_{us}|f_+(0)$ and $|V_{us}|$ values are to be compared to predictions obtained by imposing the unitary condition on the CKM matrix, and taking the latest values of $|V_{ud}| = 0.9738 \pm 0.0003$ [16] and $|V_{ub}| = (3.6 \pm 0.7) \times 10^{-3}$ [2]:

$$|V_{us}|_{unitary}f_+(0) = 0.2185 \pm 0.0022, \quad (20)$$

$$|V_{us}|_{unitary} = 0.2274 \pm 0.0013. \quad (21)$$

As shown in Fig. 10, these theoretical predictions are in good agreement with the results presented in Eq. (19). The result is in good agreement with the unitarity of the CKM mass-mixing matrix.

7.2 $\Gamma(K_{\mu 3})/\Gamma(K_{e 3})$

The consistency between the width ratio for the semileptonic decays already presented in Eq. (14) and the world average for the linear form factors parameters, λ_+ and λ_0 [2], can be tested. The band in Fig. 9 corresponds to the predictions for $\mathcal{R}_{K_{\mu 3}/K_{e 3}}$ assuming $\mu - e$ universality, Eq. (6), with the λ_+ and λ_0 values given for K^\pm in the PDG of 2006 [2]. Using Eq. (6), $\mathcal{R}_{K_{\mu 3}/K_{e 3}}$ is predicted to be 0.6682 ± 0.0017 . The result for $\mathcal{R}_{K_{\mu 3}/K_{e 3}}$ suggests a lower value for λ_0 than the current world average for K^\pm [2], as found in recent measurements from K_L [2] decays.

$\mu - e$ universality can be tested using the $\mathcal{R}_{K_{\mu 3}/K_{e 3}}$ ratio and Eq. (7). The result shown in Eq. (14) implies that $g_\mu f_+^\mu(0)/g_e f_+^e(0)$ is 0.99 ± 0.01 , which is consistent with unity within the experimental error.

Conclusion

The measured ratios of the decay rates for the charged kaon semileptonic decays are found to be:

$$\mathcal{R}_{K_{e 3}/K_{2\pi}} = 0.2496 \pm 0.0009(stat) \pm 0.0004(syst), \quad (22)$$

$$\mathcal{R}_{K_{\mu 3}/K_{2\pi}} = 0.1637 \pm 0.0006(stat) \pm 0.0003(syst), \quad (23)$$

$$\mathcal{R}_{K_{\mu 3}/K_{e 3}} = 0.656 \pm 0.003(stat) \pm 0.001(syst). \quad (24)$$

Using the current experimental knowledge of the $K_{2\pi}$ branching ratio, this leads to branching fractions of $Br(K_{e 3}) = 0.05221 \pm 0.00036$ and $Br(K_{\mu 3}) = 0.03425 \pm 0.00024$. This exceeds the PDG value [2] in both cases.

Combining these results, we find $|V_{us}|f_+(0) = 0.2197 \pm 0.0012$, in good agreement with the CKM unitary prediction.

$\mathcal{R}_{K_{\mu 3}/K_{e 3}}$ is in reasonable agreement with the semi-empirical predictions and the error is improved compared to the current world average.

Acknowledgments

It is a pleasure to thank the technical staff of the participating laboratories, universities and affiliated computing centers for their efforts in the construction of the NA48 apparatus, in the operation of the experiment, and in the processing of the data. We would also like to thank Gino Isidori and Vincenzo Cirigliano for important discussions and C. Gatti for his important contribution to the calculation of radiative corrections.

| Decay type | Raw number of events (N_i) | Acceptance \times particle ID ($Acc_i \times \epsilon_{trackID}$) | Backgrounds/Signal (Δ_i) | Trigger Efficiency ($Trig_i$) |
|--------------|-----------------------------------|--------------------------------------------------------------------------|--------------------------------------|------------------------------------|
| K_{e3}^+ | 56,196 | 0.0690 ± 0.0001 | $(0.0202 \pm 0.0008)\%$ | 0.9990 ± 0.0005 |
| K_{e3}^- | 30,898 | 0.0688 ± 0.0001 | $(0.0211 \pm 0.0010)\%$ | 0.9982 ± 0.0008 |
| $K_{\mu3}^+$ | 49,364 | 0.0927 ± 0.0001 | $(0.2215 \pm 0.0079)\%$ | 0.9986 ± 0.0006 |
| $K_{\mu3}^-$ | 27,525 | 0.0925 ± 0.0001 | $(0.2175 \pm 0.0077)\%$ | 0.9988 ± 0.0007 |
| $K_{2\pi}^+$ | 461,837 | 0.1418 ± 0.0001 | $(0.2945 \pm 0.0058)\%$ | 0.9987 ± 0.0002 |
| $K_{2\pi}^-$ | 256,619 | 0.1412 ± 0.0001 | $(0.2932 \pm 0.0058)\%$ | 0.9990 ± 0.0002 |

Table 1: Summary of information used to extract the branching ratio, where $track = e^\pm, \mu^\pm, \pi^\pm$ for $i = K_{e3}^\pm, K_{\mu3}^\pm, K_{2\pi}^\pm$.

| Contributing channel | K^+ | K^- |
|-------------------------|-------------------------|-------------------------|
| K_{e3} | | |
| $K_{\pi^\pm\pi^0\pi^0}$ | $(0.0131 \pm 0.0007)\%$ | $(0.0139 \pm 0.0009)\%$ |
| $K_{2\pi}$ | $(0.0071 \pm 0.0003)\%$ | $(0.0072 \pm 0.0004)\%$ |
| $K_{\mu3}$ | | |
| $K_{\pi^\pm\pi^0\pi^0}$ | $(0.1598 \pm 0.0045)\%$ | $(0.1599 \pm 0.0046)\%$ |
| $K_{2\pi}$ | $(0.0617 \pm 0.0064)\%$ | $(0.0576 \pm 0.0061)\%$ |
| $K_{2\pi}$ | | |
| $K_{\mu3}$ | $(0.2848 \pm 0.0058)\%$ | $(0.2846 \pm 0.0058)\%$ |
| K_{e3} | $(0.0097 \pm 0.0007)\%$ | $(0.0090 \pm 0.0008)\%$ |

Table 2: Percentage of background expected from Monte Carlo simulation for K_{e3} , $K_{\mu3}$ and $K_{2\pi}$ from the main contributors to their total background.

| Parameter Changed | $\frac{\partial \mathcal{R}_{Ke3/K2\pi}}{\partial \lambda_i}$ | $\frac{\partial \mathcal{R}_{K\mu3/K2\pi}}{\partial \lambda_i}$ | $\frac{\partial \mathcal{R}_{K\mu3/Ke3}}{\partial \lambda_i}$ |
|-------------------|---------------------------------------------------------------|-----------------------------------------------------------------|---------------------------------------------------------------|
| λ'_+ | -0.160 | -0.076 | 0.113 |
| λ''_+ | -0.319 | -0.204 | 0.021 |
| λ_0 | — | -0.048 | -0.192 |

Table 3: Dependence of the $\mathcal{R}_{Ke3/K2\pi}$, $\mathcal{R}_{K\mu3/K2\pi}$ and $\mathcal{R}_{K\mu3/Ke3}$ measurements, when changing the form factor parameter, λ_i , by \pm one sigma, and maintaining the other form factor parameters constant.

| | $\mathcal{R}_{Ke3/K2\pi}$ | | $\mathcal{R}_{K\mu3/K2\pi}$ | | $\mathcal{R}_{K\mu3/Ke3}$ | |
|---------------------------------|---------------------------|---------|-----------------------------|---------|---------------------------|---------|
| | K^+ | K^- | K^+ | K^- | K^+ | K^- |
| Central value | 0.2504 | 0.2481 | 0.1636 | 0.1639 | 0.6532 | 0.6606 |
| Statistical error | 0.0011 | 0.0015 | 0.0008 | 0.0010 | 0.0040 | 0.0055 |
| Total systematic error | 0.0005 | 0.0006 | 0.0004 | 0.0004 | 0.0016 | 0.0018 |
| Accept. \times Part-ID num. | 0.00041 | 0.00047 | 0.00017 | 0.00017 | 0.00067 | 0.00068 |
| Accept. \times Part-ID denom. | 0.00021 | 0.00021 | 0.00014 | 0.00014 | 0.00106 | 0.00126 |
| Trigger efficiency in num. | 0.00013 | 0.00020 | 0.00010 | 0.00011 | 0.00039 | 0.00046 |
| Trigger efficiency in denom. | 0.00005 | 0.00005 | 0.00003 | 0.00003 | 0.00033 | 0.00053 |
| Background subtraction | 0.00001 | 0.00001 | 0.00002 | 0.00002 | 0.00005 | 0.00005 |
| Uncertainty in form factor | 0.00010 | | 0.00010 | | 0.00029 | |
| Uncertainty in f. f. model | 0.00009 | | 0.00026 | | 0.00086 | |

Table 4: Summary of the statistical and systematic uncertainties for the $\mathcal{R}_{Ke3/K2\pi}$, $\mathcal{R}_{K\mu3/K2\pi}$ and $\mathcal{R}_{K\mu3/Ke3}$ measurements.

| Decay Channel | Branching Fraction Br | Phase Space Integral I_K^ℓ | Radiative Correction[4, 5, 6] | | $ V_{us} f_+(0)$ |
|---------------|----------------------------|------------------------------------|-------------------------------|------------------------|---------------------|
| | | | $\delta_{SU(2)}^\ell(\%)$ | $\delta_{EM}^\ell(\%)$ | |
| K_{e3} | 0.0522 ± 0.0004 | 0.1591 ± 0.0012 | 2.31 ± 0.22 | 0.03 ± 0.10 | 0.2204 ± 0.0012 |
| $K_{\mu3}$ | 0.0343 ± 0.0002 | 0.1066 ± 0.0008 | 2.31 ± 0.22 | 0.20 ± 0.20 | 0.2177 ± 0.0013 |

Table 5: Inputs to Eq. (3) and results for $|V_{us}|f_+(0)$. By assuming unitarity, the prediction of $|V_{us}|f_+(0)$ for charged kaons is 0.2185 ± 0.0022 .

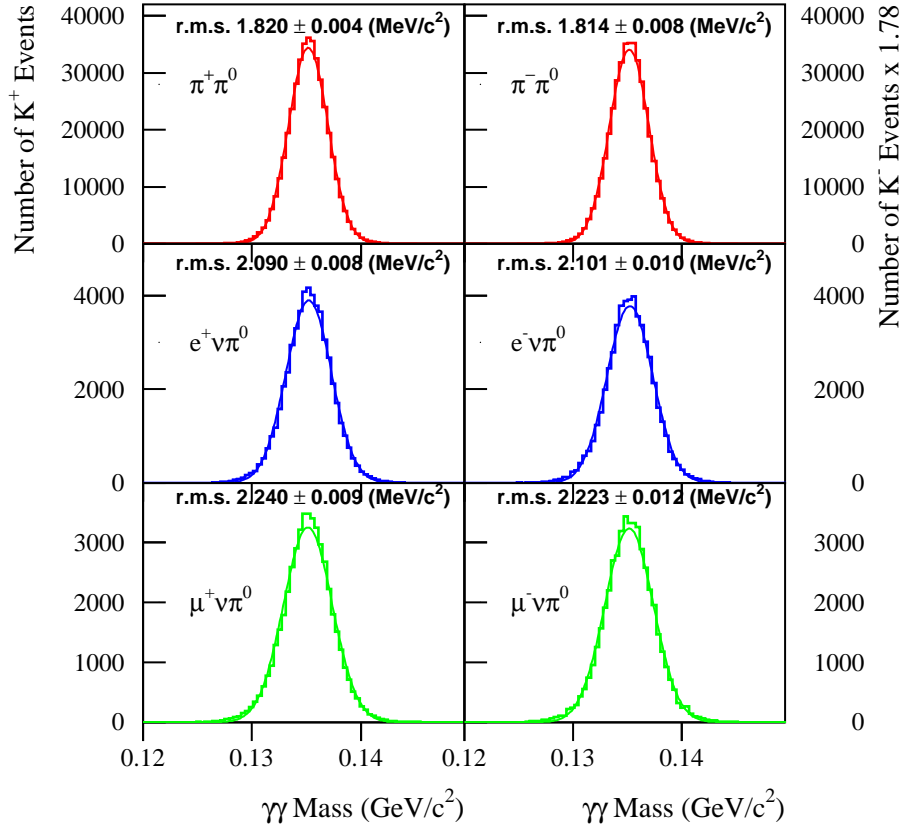


Figure 1: The three final states are characterized by different average photon energies and acceptance. This fact is reflected into the variation of the root mean square (r.m.s.) of the $\gamma\gamma$ invariant mass distribution. The solid curves represent Gaussian fits with the particular r.m.s. value noted in each plot. These variations however are small enough and do not introduce systematics in the normalisation of the results. A clear π^0 signal is shown in all channels after applying the full event selection. The factor of 1.78 corresponds to the ratio of K^+ to K^- flux in the beamline.

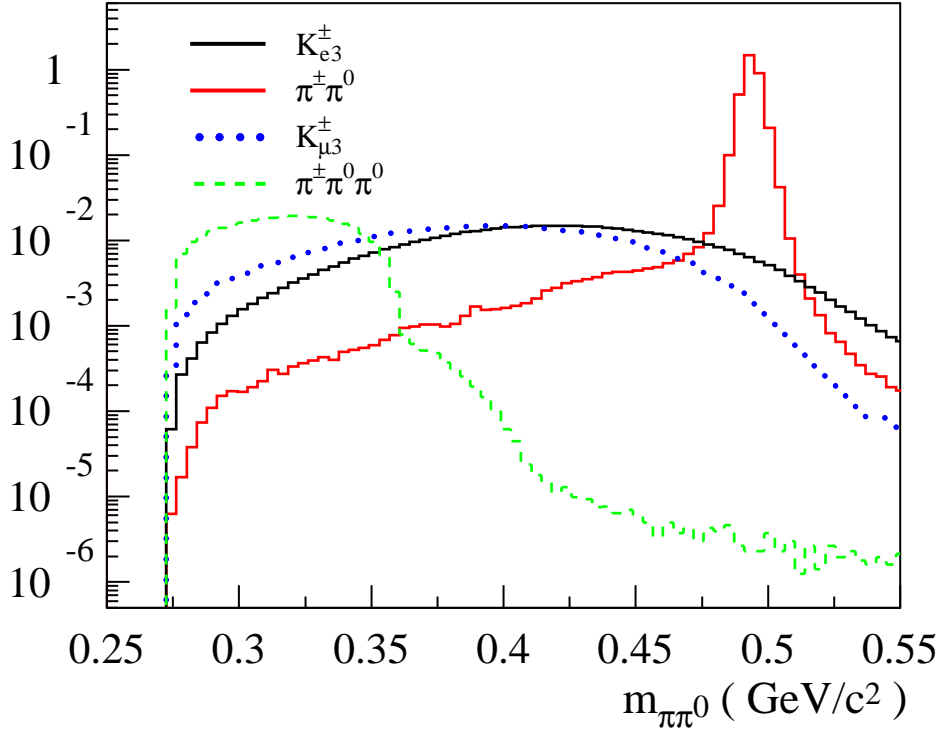


Figure 2: Monte Carlo simulation for K_{e3} , $K_{\mu3}$, $K_{3\pi}$ and $K_{2\pi}$. These are the distributions of the reconstructed invariant mass of the two best photons and the track without applying particle identification, and under the assumption that the two photons come from a π^0 decay and the track is a π^\pm .

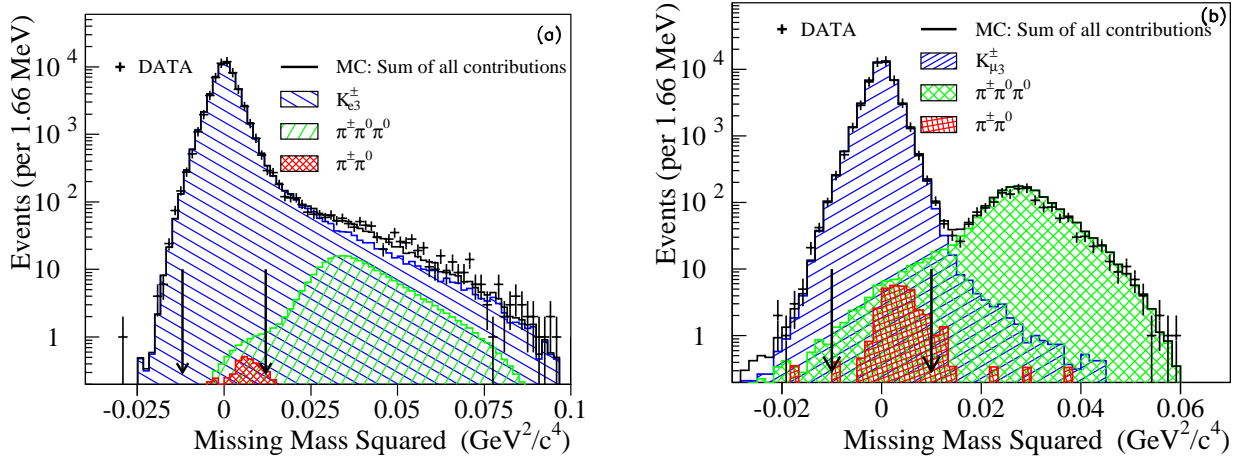


Figure 3: Data and Monte Carlo comparison for the reconstructed missing mass squared, m_ν^2 , for (a) K_{e3} and (b) $K_{\mu3}$ candidates. Only the information from the charged lepton and the π^0 is used and extra photons are ignored, if present in the event. A good description is found after summing the Monte Carlo prediction for the signal and the various background components. Arrows indicate the allowed range in the event selection. The charged kaon energy is assumed to be 60 GeV.

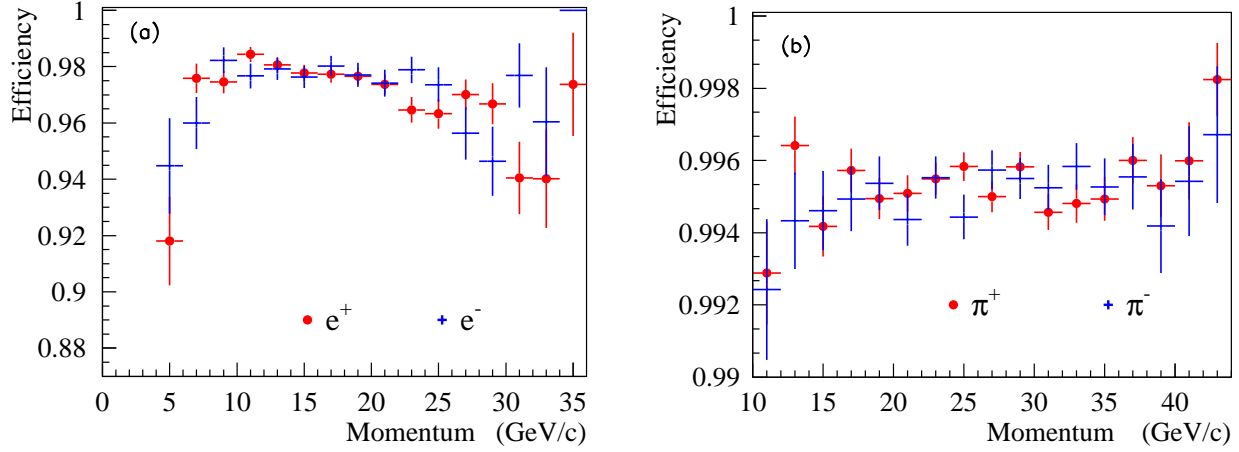


Figure 4: The E/pc particle identification efficiency for (a) electrons and (b) charged pions from clean subsamples of K_{e3} and $K_{2\pi}$ decays respectively. These data samples have more stringent requirements on the kaon mass, the missing mass and the transverse momentum of the track.

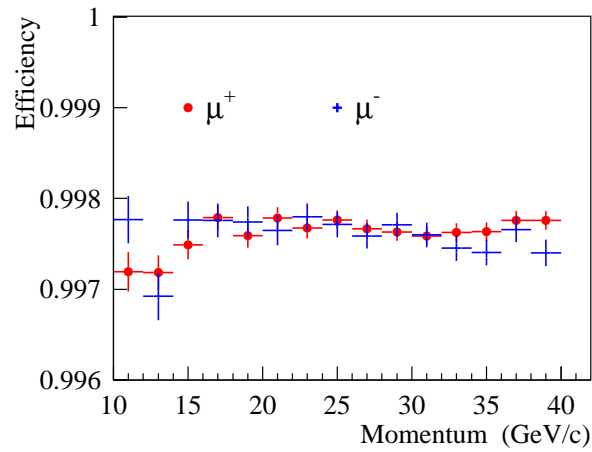


Figure 5: Particle identification efficiency for muons measured using a sample obtained from $K^\pm \rightarrow \mu^\pm \nu$ decays.

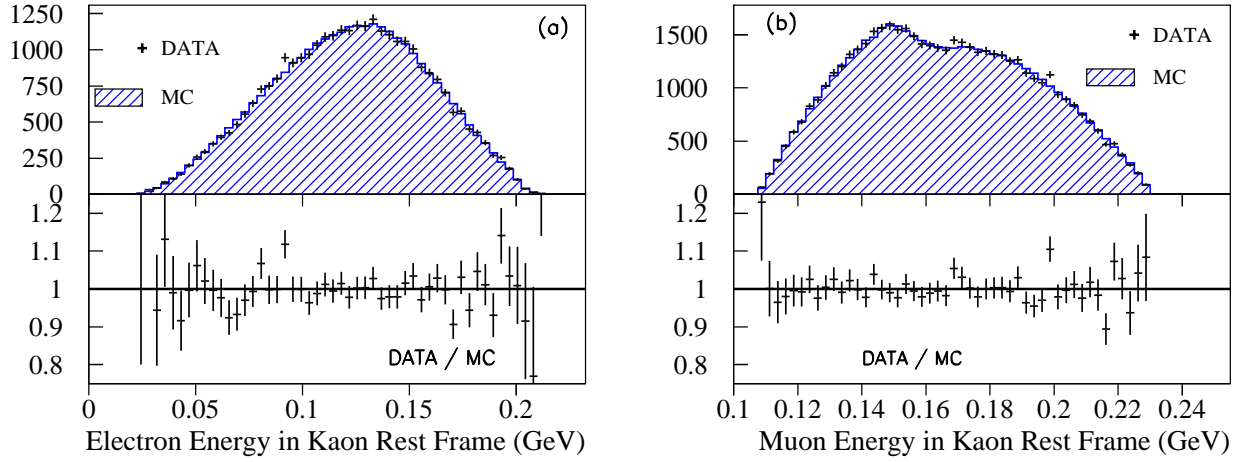


Figure 6: Comparison of the (a) electron and (b) muon energy in the kaon rest frame for K_{e3} and $K_{\mu 3}$ events. Ratio of the Data over Monte Carlo is given in the lower plots.

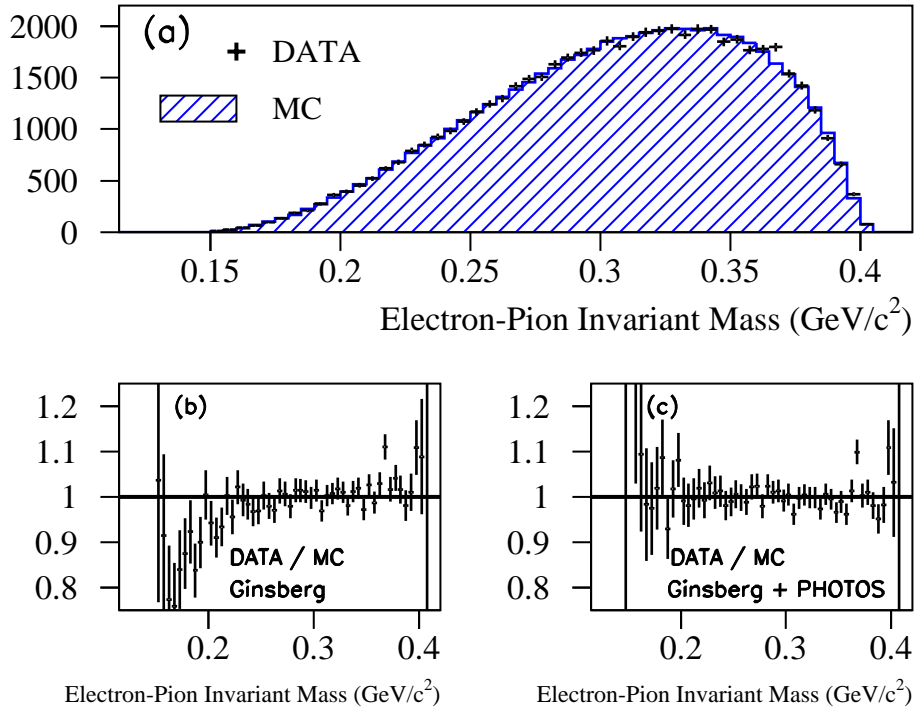


Figure 7: (a) Comparison of the electron and the π^0 invariant mass distribution for K_{e3} events. Ratio of the Data over Monte Carlo given in the lower plots for Monte Carlo generated with corrections to the Dalitz distributions for virtual effects[5] and real photons due to bremsstrahlung[10] (c) is in good agreement, while (b) only correcting the Dalitz distributions for virtual effects[5] and ignoring the $K_{e3\gamma}$ contribution fails to described the low mass region.

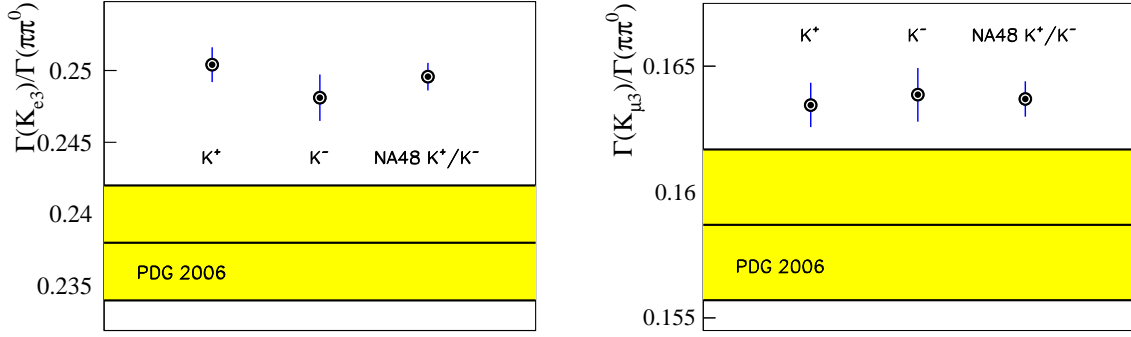


Figure 8: $\mathcal{R}_{Ke3/K2\pi}$ and $\mathcal{R}_{K\mu3/K2\pi}$ results compared to the corresponding PDG value [2].

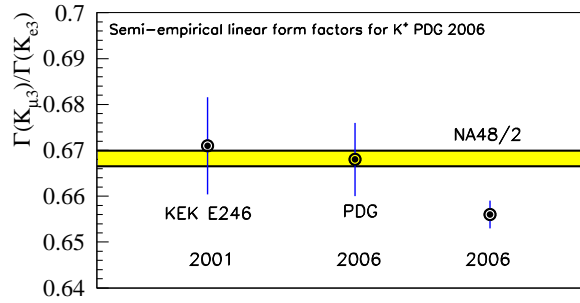


Figure 9: $\mathcal{R}_{K\mu3/Ke3}$ results compared to KEK-246 results [17], the corresponding PDG value of 2006 [2] and to the predictions assuming $\mu - e$ universality, Eq. (6), with the λ_+ and λ_0 values given for K^\pm in the PDG of 2006 [2].

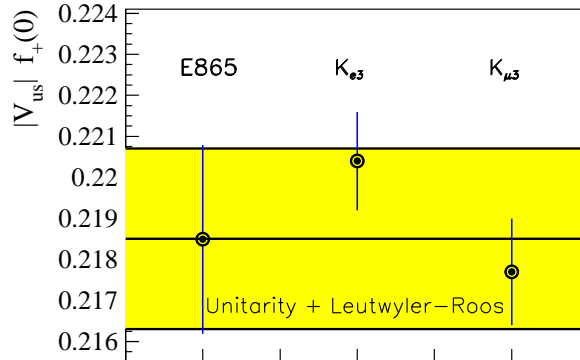


Figure 10: Comparison of the NA48 measurement of $|V_{us}| f_+(0)$ from K_{e3} and $K_{\mu3}$ data, and the K_{e3} BNL-E865 result [13]. The theoretical prediction shown is obtained assuming unitarity of the CKM matrix V_{ud} , using the PDG values for V_{ud} and V_{ub} as input, and using the choice of $f_+(0)$ as described in the text.

References

- [1] H. Leutwyler and M. Roos, *Z. Phys. C* **25** (1984) 91
- [2] W.-M. Yao *et al.* [Particle Data Group], *J. Phys. G* **33** (2006) 1; [<http://pdg.lbl.gov>]
- [3] J. Bijnens, G. Colangelo, G. Ecker and J. Gasser [arXiv:hep-ph/9411311]; 2nd DAPHNE Physics Handbook (1994) 315-389
- [4] V. Cirigliano *et al.*, *Eur. Phys. J. C* **35** (2004) 53 [arXiv:hep-ph/0401173];
V. Cirigliano *et al.*, *Eur. Phys. J. C* **23** (2002) 121 [arXiv:hep-ph/0110153]
- [5] E. S. Ginsberg, *Phys. Rev. D* **1** (1970) 229; *Phys. Rev.* **162** (1967) 1570 [Erratum-
ibid. **187** (1969) 2280]
- [6] E. Blucher *et al.*, Proceedings of the CKM 2005 Workshop (WG1), UC San Diego, 15-18 March 2005 [arXiv:hep-ph/0512039]
- [7] G.D. Barr *et al.*, *Nucl. Instrum. Meth. A* **370** (1996) 413; G. Unal, NA48 Collaboration, in: IX International Conference on Calorimetry, October 2000, Annecy, France [arXiv:hep-ex/0012011]
- [8] GEANT Detector Description and Simulation Tool, CERN Program Library Long Write-up W5013 (1994)
- [9] D.C. Carey, "TURTLE (Trace Unlimited Rays Through Lumped Elements) A Computer Program for Simulating Charged Particle Beam Transport Systems," Fermi National Accelerator Laboratory Report No. NAL-64, 45 pages (1978)
- [10] E. Barberio and Z. Was, *Comput. Phys. Com.* **79** (1994) 291; P. Golonka, Z. Was, *Eur. Phys. J. C* **45** (2006) 97 [arXiv:hep-ph/0506026]
- [11] C. Gatti, *Eur. Phys. J. C* **45** (2006) 417 [arXiv:hep-ph/0507280]
- [12] Calculated from the ratio of the two branching ratios in [2], ignoring correlations
- [13] A. Sher *et al.*, *Phys. Rev. Lett.* **91** (2003) 261802 [arXiv:hep-ex/0305042]
- [14] A. Czarnecki, W. J. Marciano and A. Sirlin, *Phys. Rev. D* **70** (2004) 093006 [arXiv:hep-ph/0406324]
- [15] A. Sirlin, *Nucl. Phys. B* **196** (1982) 83
- [16] W. J. Marciano and A. Sirlin, *Phys. Rev. Lett.* **96** (2006) 032002 [arXiv:hep-ph/0510099]
- [17] K. Horie *et al.*, *Phys. Lett. B* **513** (2001) 311